Cancer Stem Cells in Head and Neck Cutaneous Squamous Cell Carcinoma Express Cathepsins

Therese Featherston, BBiomedSc(Hons)*
Helen D. Brasch, MBChB, FRCPA*
Sam D. Siljee, MBChB*
Bede van Schaijik, BTech(Hons)*
Josie Patel, MSc*
Jennifer de Jongh, BBiomedSc*
Reginald W. Marsh, PhD*†
Tinte Itinteang, MBBS, PhD*
Swee T. Tan, MBBS, FRACS, PhD*‡§

Background: Cancer stem cell (CSC) subpopulations within moderately differentiated head and neck cutaneous squamous cell carcinoma (MDHNcSCC) express the components of the renin–angiotensin system (RAS). This study investigated the expression of cathepsins B, D, and G, which constitute bypass loops of the RAS, by CSCs in MDHNcSCC.

Methods: Immunohistochemical staining was performed on MDHNcSCC tissue samples from 15 patients to determine the expression of cathepsins B, D, and G. Co-localization of these cathepsins with the embryonic stem cell markers Octamer-binding transcription factor 4 (OCT4) and c-MYC was investigated with immunofluorescence staining. Reverse transcription quantitative polymerase chain reaction was performed on 5 MDHNcSCC tissue samples to investigate transcript expression of cathepsins B, D and G. Western blotting and enzymatic activity assays were performed on 5 MDHNcSCC tissue samples and 6 MDHNcSCC-derived primary cell lines to confirm protein expression, transcript expression, and functional activity of these cathepsins, respectively.

Results: Immunohistochemical staining demonstrated the expression of cathepsins B, D, and G in all MDHNcSCC tissue samples. Immunofluorescence staining showed localization of cathepsins B and D to the c-MYC+ CSC subpopulations and the OCT4+ CSC subpopulations within the tumor nests and the peritumoral stroma. Cathepsin G was expressed on the tryptase+/c-MYC+ cells within the peritumoral stroma. Reverse transcription quantitative polymerase chain reaction demonstrated transcript expression of cathepsins B, D and G in the MDHNcSCC tissue samples. Western blotting and enzymatic activity assays confirmed protein expression and functional activity of cathepsins B and D in the MDHNcSCC tissue samples and MDHNcSCC-derived primary cell lines, respectively.

Conclusions: Cathepsins B, D, and G are expressed in MDHNcSCC with functionally active cathepsins B and D localizing to the CSC subpopulations, and cathepsin G is expressed by mast cells, suggesting the potential use of cathepsin inhibitors in addition to RAS blockade to target CSCs in MDHNcSCC. *(Plast Reconstr Surg Glob Open 2020;8:e3042; doi: 10.1097/GOX.0000000000003042; Published online 19 August 2020.)*

INTRODUCTION

Cutaneous squamous cell carcinoma (cSCC), the second most common nonmelanoma skin cancer[1] accounting

Related Digital Media are available in the full-text version of the article on www.PRSGlobalOpen.com.

for 15%–25%, is increasing rapidly worldwide.[2] Risk factors for cSCC include childhood and adolescent exposure to ultraviolet radiation, immunosuppression, and chronic ulcers.[2]

cSCC commonly affects the head and neck,[3] with a 1.9%–2.6% risk of metastasis, most commonly to parotid and neck nodes with known risk factors, including perineural invasion, lymphovascular invasion, poor histological differentiation, and certain anatomic subsites.[1,2] Current treatment for metastatic head and neck cutaneous SCC (HNcSCC) involves radical surgery and adjuvant radiotherapy,[3] with a 5-year survival of 48%.[3]

Cancer stem cells (CSCs), the proposed origin of cancer, possess the ability to both self-renew and form downstream progenitor cancer cells with more limited tumorigenicity.[4] CSCs are highly tumorigenic compared with cancer cells, which form the bulk of the tumor,[5] suggesting the presence of a hierarchy.[6–8] Overexpression of embryonic stem cell markers is associated with increased tumor size and invasion, local recurrence, and metastasis.[4]

CSCs have been identified in many cancer types, including oral cavity SCC (OCSCC) of different subsites,[9–11] glioblastoma,[12] renal clear cell carcinoma,[13] primary[14] and metastatic[15] colon adenocarcinoma, and metastatic malignant melanoma.[16,17]

CSCs have been proposed as a novel therapeutic target,[5] with recent studies investigating different CSC-surface marker–targeted therapies and CSC-directed immunotherapy.[18,19]

Expression of components of the renin–angiotensin system (RAS) by CSCs has been demonstrated in different cancer types, including glioblastoma,[20] OCSCC,[21–23] metastatic colon adenocarcinoma,[15] and metastatic malignant melanoma,[24] suggesting the potential of targeting CSCs by modulating the RAS.[25,26]

Using induced embryonic stem cell (ESC) markers Octamer-binding transcription factor 4 (OCT4), sex determining region Y-box 2 (SOX2), Krüppel-like factor 4 (KLF4) and c-MYC, we have recently identified 4 CSC subpopulations within moderately differentiated HNcSCC (MDHNcSCC): an OCT4+/NANOG+/SOX2+/KLF4+/c-MYC+ subpopulation within the tumor nests (TNs), the peritumoral stroma (PTS), and the endothelium of the microvessel within the PTS, and an OCT4+/NANOG−/SOX2+/KLF4+/c-MYC+ subpopulation solely within the PTS.[27] These primitive cells express components of the RAS: prorenin receptor (PRR), angiotensin-converting enzyme (ACE), angiotensin receptor 1 (AT$_1$R), and angiotensin receptor 2 (AT$_2$R).[28]

The RAS is a hormonal system classically associated with blood pressure and body fluid regulation; however, there is increasing evidence for its role in tumorigenesis.[29,30] The RAS promotes cancer cell proliferation, survival, metastasis, and angiogenesis.[31] Angiotensinogen is converted to angiotensin I (ATI) by renin, which is the active form of prorenin.[30] Both renin and prorenin bind PRR.[29] ATI is then cleaved by ACE to form angiotensin II, which acts upon binding to AT$_1$R and AT$_2$R.[30] AT$_1$R promotes angiogenesis, proliferation, and pro-inflammation, whereas AT$_2$R antagonizes these functions.[29]

The production of the peptides of the RAS involves many alternative signaling pathways, including enzymes such as cathepsins B, D, and G.[32] Cathepsin B is a lysosomal cysteine protease that processes that cleaves inactive prorenin to renin.[33] Cathepsin D is an aspartyl protease that converts angiotensinogen to ATI, and is functionally homologous to renin.[34] Cathepsin G, a serine protease, processes angiotensinogen and ATI to form angiotensin II and is functionally homologous to ACE.[35] These cathepsins constitute bypass loops for the RAS and have been identified in different tumor types, including infantile hemangioma (IH),[32] glioblastoma,[36] oral tongue SCC,[37] and metastatic colon adenocarcinoma.[38]

Increased expression of cathepsins has been observed in a wide range of cancer types,[29,39] including head and neck cancer.[40–42] Increased expression of cathepsins B and D have been associated with tumor progression, including cellular proliferation and differentiation, and tumor invasion and metastasis,[39,43] and increased risk of local recurrence and metastasis.[39]

This study investigated expression of cathepsins B, D, and G using immunohistochemical staining and their localization to the CSC subpopulations within human MDHNcSCC using immunofluorescence staining. Western blotting (WB) and reverse transcription quantitative polymerase chain reaction (RT-qPCR) were used to confirm their protein and mRNA expression, respectively. Enzymatic activity assays (EAAs) were used to investigate their functional activity.

MATERIALS AND METHODS

MDHNcSCC Tissue Samples

MDHNcSCC tissue samples from 10 male and 5 female patients aged 42–99 years (mean, 76.3 years), including those used in the previous studies,[27,28] were sourced from the Gillies McIndoe Research Institute Tissue Bank for this study. The Central Regional Health and Disability Ethics Committee approved this study (Ref. 12/CEN/74). Written consent was obtained from all participants. (**See table, Supplemental Digital Content 1**, which shows the patient demographics and anatomic site of their head and neck cSCC, **http://links.lww.com/PRSGO/B447**.)

MDHNcSCC-derived Primary Cell Lines

Primary cell lines were derived from 6 fresh MDHNcSCC tissue samples from the original cohort of 15 patients. The samples were cultured within a Matrigel (cat.#354234; Corning, Tewksbury, Maine) explant and extracted following their abundant growth.[27] The extracted cells were grown and passaged in DMEM medium (cat.#10569010; Thermo Fisher Scientific, Waltham, Mass.) supplemented with 1% fetal calf serum (cat.#10091148; Thermo Fisher Scientific), 5% mTeSR (cat.#85850; STEMCELL Technologies, Vancouver, British Columbia, Canada), 1% penicillin–streptomycin (cat.#15140122; Thermo Fisher Scientific), and 0.2% gentamicin/amphotericin B (cat.#R01510; Thermo Fisher Scientific). All cultures were maintained in a humidified 37°C incubator with 5% CO_2. All primary cells used in the experiments were passages 6–8.

Immunohistochemical and Immunofluorescence Staining

Hematoxylin and eosin staining was performed on 4-μm–thick, formalin-fixed, paraffin-embedded MDHNcSCC consecutive sections from 15 patients to confirm the presence of the tumor, and appropriate histologic grading was carried out by an anatomical pathologist. Immunohistochemical staining was then performed with primary antibodies for cathepsin B (1:1000; cat.#sc-6490-R; Santa Cruz Biotechnology, Dallas, TX), cathepsin D (1:200; cat.#NCL-CDm; Leica Biosystems, Nussloch, Germany), cathepsin G (1:200; cat.#sc-33206; Santa Cruz), OCT4 (1:30; cat.#309M-16; Cell Marque, Rocklin, Calif.), c-MYC (1:1000; ca#9E10; Abcam, Cambridge, United Kingdom), and tryptase (1:300; cat.#NCL-MCTRYP-428; Leica Biosystems), with 3,3′-diaminobenzidine as the chromogen. All immunohistochemical-stained slides were mounted in Dako Mounting Medium (cat.#CS703; Dako, Santa Clara, Calif.).

Immunofluorescence dual staining was performed on 2 representative MDHNcSCC tissue samples from the original cohort of 15 patients to determine coexpression of cathepsin proteins with CSC subpopulations and tryptase. ESC markers, used for identifying CSC subpopulations, were c-MYC and OCT4.[27] Vectafluor Excel anti-mouse 488 (ready-to-use; cat.#DK-2488; Vector Laboratories, Burlingame, Calif.) and Alexa Fluor anti-rabbit 594 (1:500; cat.#A-21207; Life Technologies, Carlsbad, Calif.) were used to detect the combinations. All immunofluorescence slides were mounted in Vecta Shield Hardset mounting medium with 4′,6′-diamino-2-phenylindole (cat.#H-1500; Vector Laboratories).

Human tissues used as positive controls for primary antibodies were placenta (for cathepsin B),[37] breast adenocarcinoma (for cathepsin D),[37] and tonsil (for cathepsin G).[44] For immunohistochemical staining, matched isotype controls (ready-to-use; cat.#IR600 and ready-to-use; cat.#IR750; Dako) were used on MDHNcSCC sections as negative controls. For immunofluorescence staining, primary isotype mouse (ready-to-use; cat.#IR750; Dako) and rabbit (ready-to-use; cat.#IR600, Dako) controls were used on MDHNcSCC tissue sections as negative controls.

All antibodies were diluted with BOND primary antibody diluent (cat.#AR9352; Leica). All immunohistochemical and immunofluorescence staining was performed on a Leica BOND RX autostainer.

Image Capture and Analysis

Immunohistochemical-stained slides were viewed and imaged on an Olympus BX53 light microscope fitted with an Olympus SC100 digital camera, and processed with cellSens 2.0 software (Olympus, Tokyo, Japan). Immunofluorescence slides were viewed and imaged on an Olympus FV1200 confocal laser-scanning microscope (Olympus). All immunofluorescence images were processed with cellSens Dimension software (v1.11) using a 2D deconvolution algorithm (Olympus).

Western Blotting

Total protein was extracted and precipitated from 5 snap-frozen MDHNcSCC tissue samples and 6 MDHNcSCC-derived primary cell lines from the original cohort of 15 patients. The protein was separated by SDS-PAGE and transferred to a PVDF membrane.[28] Detection of protein was performed on the iBind Flex (cat.#SLF200; Thermo Fisher Scientific) using the primary antibodies for cathepsin B (1:250; cat.#sc-6490-R; Santa Cruz), cathepsin D (1:250; cat.#sc-6486; Santa Cruz), cathepsin G (1:500; cat.#ab197354; Abcam), and α-tubulin (1:1000; cat.#62204; Thermo Fisher Scientific). Secondary antibodies (all from Life Technologies) used were goat anti-rabbit Alexa Fluor 647 (1:2000; cat.#A-21244) for cathepsin B, chicken anti-goat Alexa Fluor 647 (1:2000; cat.#A-21469) for cathepsin D, donkey anti-mouse Alexa Fluor 488 (1:2000; cat.#A-21202) for α-tubulin, and goat anti-rabbit horseradish peroxidase (HRP) (1:2000; cat.#ab6721; Abcam) for the detection of cathepsin G in the cell lines. For the detection of cathepsin G in the tissues, a tertiary cascade consisting of rabbit anti-goat Superclonal biotin-conjugated secondary antibody (1:20000; cat.#A27013; Thermo Fisher Scientific) followed by a Pierce Streptavidin Poly HRP (1:5000; cat.#21140; Thermo Fisher Scientific) at 4°C for 10 minutes was used. Clarity Western ECL (cat.#1705061; Bio-Rad, Hercules, Calif.) was used as the substrate for visualizing HRP-detected protein bands. The ChemiDoc MP Imaging System (Bio-Rad) and Image Lab 6.0 software (Bio-Rad) were used for band detection and analysis.

Snap-frozen human tonsil was used as a positive control for cathepsin B[38] and cathepsin D.[38] A recombinant cathepsin G protein (cat.#H00001511-Q01; Novus Biologicals, Littleton, Colo.) was used as a positive control for cathepsin G. Matched mouse (1:500; cat.#ab18443; Abcam) and rabbit (1:500; cat.#ab171870; Abcam) isotype controls were used as appropriate negative controls. All primary and secondary antibodies were diluted in iBind Flex FD solution (cat.#SLF2019; Thermo Fischer Scientific).

Enzymatic Activity Assays

The functional activity of cathepsins B and D in 5 snap-frozen MDHNcSCC tissue samples and 5 of the 6 MDHNcSCC-derived primary cell lines used for WB was determined using EAA kits for cathepsin B (cat.#ab65300; Abcam) and cathepsin D (cat.#ab65302; Abcam). All steps of the procedure were performed as described elsewhere.[37] Fluorescence was measured in a black, clear-bottomed 96-well plate (cat.#3631; Corning) using the Varioskan Flash plate reader (Thermo Fisher Scientific). Human tonsil and denatured tonsil lysates were used as appropriate positive and negative controls, respectively.[37]

RT-qPCR

Total RNA was extracted from 20 mg sections of each of the 5 snap-frozen MDHNcSCC tissue samples from the original cohort of 15 patients. Tissue sections were homogenized using the Omni Tissue Homogenizer (Omni International, Kennesaw, Ga.) and then prepared using the RNeasy Mini Kit (cat.#74104; Qiagen, Hilden, Germany) following the manufacturer's instructions. An on-column DNase digest (cat.#79254; Qiagen) step was included to remove potentially contaminating genomic DNA. To determine RNA quantity, samples were subjected to NanoDrop 2000 spectrophotometer (Thermo Fisher Scientific) quantification.

Gene expression was analyzed in triplicate by RT-qPCR using a Rotor-Gene Multiplex RT-PCR Kit (Qiagen) on the Rotor-Gene Q (cat.#204974, Qiagen) and TaqMan gene expression assays. The primer probes used were cathepsin B (Hs00157194_m1), cathepsin D (Hs00157205_m1), cathepsin G (Hs00175195_m1), and the housekeeper genes glyceraldehyde 3-phosphate dehydrogenase (*GAPDH*) (Hs99999905_m1) and Pumilio RNA Binding Family Member 1 (*PUM1*) (Hs00206469_m1). All primers were obtained from Thermo Fisher Scientific (cat.#4331182).

Universal human reference RNA (UHR) (cat.#CLT636690; Takara, Shiga, Japan), total RNA extracted from a range of healthy adult human tissues, was used as the calibrator for the fold-change (2ΔΔCt) analysis. Nuclease-free water was added for the no template control, and RNAs from human tonsil for the cathepsin assays[45] were used as a positive control. The presence of the correctly sized bands from the endpoint amplification products was confirmed using 2% agarose gel electrophoresis (cat.#G402002; Thermo Fisher Scientific) and imaged using the ChemiDoc MP (Bio-Rad, Hercules, Calif.).

Statistical Analysis

Graphs were generated using GraphPad Prism (v8.0.2, San Diego, Calif.), with PCR results expressed as fold-change relative to UHR. A fold-change cutoff was set at 2.0 for upregulated and 0.5 for downregulated genes.

RESULTS

Histochemical and Immunohistochemical Staining

Hematoxylin and eosin staining of all 15 MDHNcSCC tissue samples confirmed the presence and appropriate histologic grading of the tumors. Immunohistochemical staining of all MDHNcSCC tissue samples showed a strong cytoplasmic expression of cathepsin B (Fig. 1A) and cathepsin D (Fig. 1B) by cells within the TNs (bold arrows), the PTS (thin arrows), and the endothelium (arrowheads) of the microvessels within the PTS. Cathepsin G (Fig. 1C) staining was confined to cells within the PTS.

Human tissues used as positive controls for cathepsins B, D, and G demonstrated expected staining patterns. [**See figure, Supplemental Digital Content 2,** which shows representative immunohistochemical-stained sections of positive human control tissues showing the expected staining pattern for cathepsin B (A, brown) in placenta, cathepsin D (B, brown) in breast carcinoma, and cathepsin G (C, brown) in tonsil. A moderately differentiated head and neck squamous cell carcinoma tissue sample was used as a negative control by using an IgG isotype control (D). Nuclei were counter-stained with hematoxylin (A–C, blue). Original magnification: ×400, **http://links.lww.com/PRSGO/B448.**]

Immunofluorescence Staining

Immunofluorescence staining was performed on 2 representative MDHNcSCC tissue samples, to determine the expression of cathepsins B, D, and G in relation to the MDHNcSCC CSC subpopulations recently identified.[27]

The c-MYC+ (Fig. 2A–C, green) CSC subpopulations within the TNs (arrows) and the PTS (arrowheads) expressed both cathepsin B (Fig. 2A, red) and cathepsin D (Fig. 2B, red). Cathepsin G (Fig. 2C, red) was expressed only by the c-MYC+ CSC subpopulations within the PTS (arrows). Cathepsin B (Fig. 2D, red) and cathepsin D (Fig. 2E, red), but not cathepsin G (Fig. 2F, red), were expressed by the OCT4+ (Fig. 2D–F, green) CSC subpopulations. Cathepsins B and D were expressed by 2 CSC subpopulations within the PTS, one expressing OCT4 (Fig. 2D, E, green, arrows) and another devoid of OCT4 (Fig. 2D, E, green, arrowheads). Cathepsin G (Fig. 2G, red) was expressed on the tryptase+ (Fig. 2G, green) mast cells, as shown in IH.[32]

Split images of Figure 2 are presented in SDC3. Minimal staining was present on the negative control confirming the specificity of the primary antibodies. [**See figure, Supplemental Digital Content 3,** which shows split immunofluorescence-stained images for cathepsin B (A, red) and c-MYC (B, green); cathepsin D (C, red) and c-MYC (D, green); cathepsin G (E, red) and c-MYC (F, green); cathepsin B (G, red) and OCT4 (H, green); cathepsin D (I, red) and OCT4 (J, green); cathepsin G (K, red) and OCT4 (L, green); and cathepsin B (M, red) and tryptase (N, green). A moderately differentiated head and neck squamous cell carcinoma tissue sample was used as a negative control (O) by using primary isotype mouse and rabbit antibodies. Cell nuclei were counter-stained with 4′,6′-diamino-2-phenylindole (A–O, blue). Original magnification: ×400. Scale bar: 20 μm, **http://links.lww.com/PRSGO/B449.**]

Fig. 1. Representative immunohistochemical-stained sections of moderately differentiated head and neck squamous cell carcinoma tissue samples demonstrating the expression of cathepsin B (A, brown) and cathepsin D (B, brown) within the tumor nests (TNs, *bold arrows*), the peritumoral stroma (PTS, *thin arrows*), and the endothelium of the microvessel (*arrowheads*) within the PTS. Expression of cathepsin G (C, brown) was confined to some cells within the PTS. Nuclei were counter-stained with hematoxylin (A–C, blue). Original magnification: ×400.
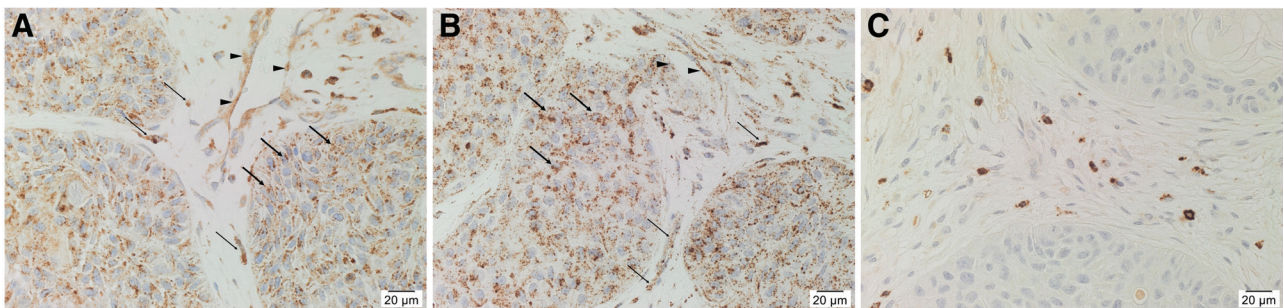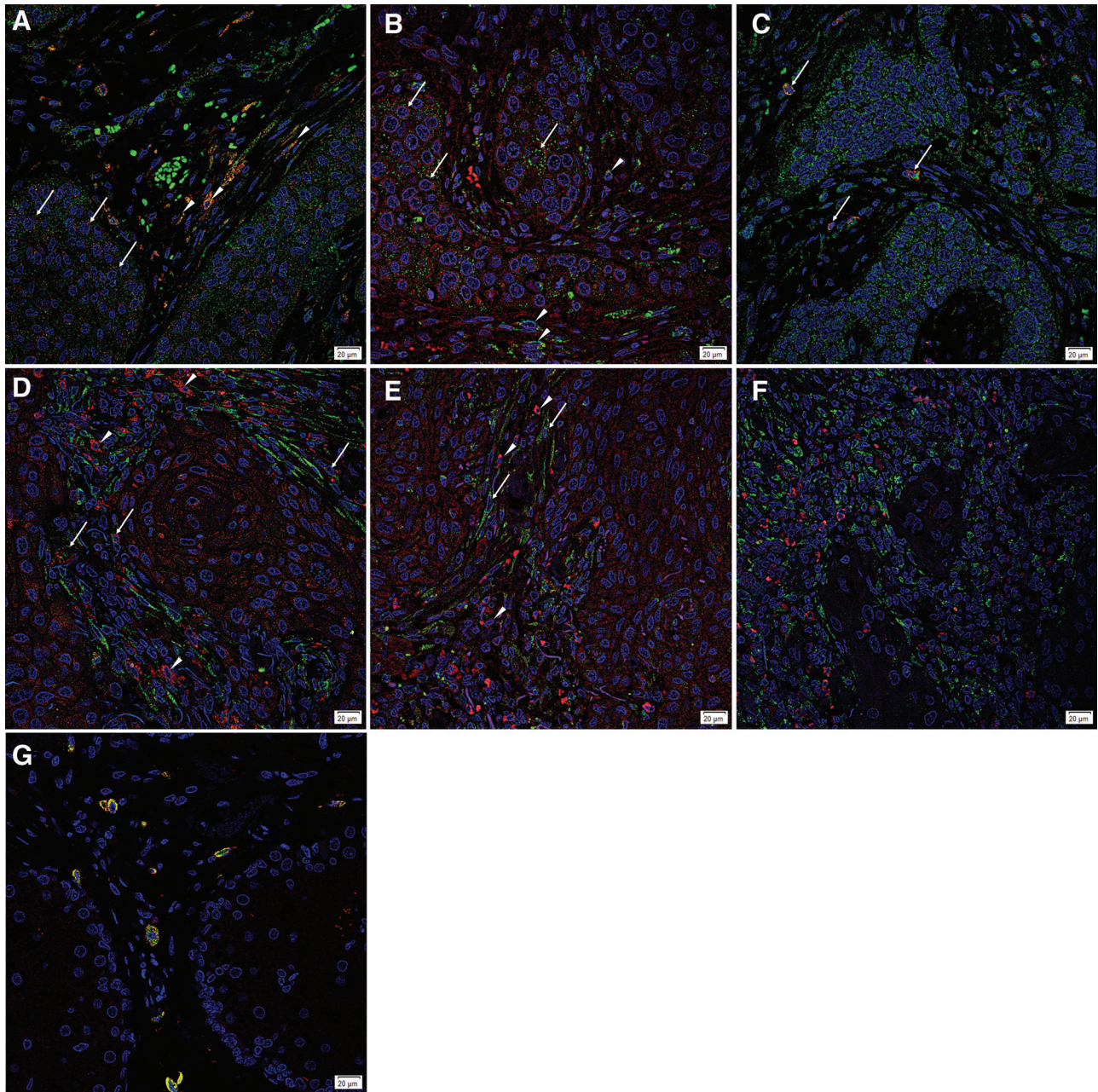
Fig. 2. Representative immunofluorescence sections of moderately differentiated head and neck squamous cell carcinoma tissue samples demonstrating expression of cathepsin B (A, D, red) by the c-MYC⁺ (A, green) cells within the tumor nests (TNs) (A, arrows), as well as cells in the peritumoral stroma (PTS) (A, arrowheads). The cells within the PTS are both OCT4⁺ (D, green, arrows) and OCT4⁻ (D, red, arrowheads). Similarly, cathepsin D (B, E, red) was also expressed by the c-MYC⁺ (B, green) cells within the TNs (B, arrows) and the PTS (B, arrowheads), as well as both the OCT4⁺ (E, green, arrows) and OCT4⁻ (E, red, arrowheads) cells of the PTS. Cathepsin G (C, F, red) was expressed by some c-MYC⁺ (C, green, arrows) cells within the PTS, but not by the OCT4⁺ (F, green) cells. Tryptase⁺ (G, green) cells within the PTS also expressed cathepsin G (G, red). All slides were counter-stained with 4′,6′-diamino-2-phenylindole. Original magnification: ×400. Scale bar: 20 μm.

Western Blotting

WB confirmed the presence of cathepsins B and D in all 5 snap-frozen MDHNcSCC tissue samples, with cathepsin B (Fig. 3A) showing the expected molecular weight of 25 kDa[46] in all 5 samples. An additional band at 45 kDa was detected in one sample, indicating the presence of procathepsin B.[46] The mature form of cathepsin D (Fig. 3B) at the expected size of 33 kDa was detected[47] in all 5 samples. Cathepsin G (Fig. 3C) was not detected in any of the 5 samples.

WB confirmed the presence of cathepsins B and D in all 6 MDHNcSCC-derived primary cell lines. Three bands at 25, 27, and 42 kDa were present for cathepsin B (Fig. 3D), confirming the presence of the mature form of cathepsin B at 25 kDa, a 25–27 kDa doublet form of mature cathepsin B, and procathepsin B at 42 kDa.[46] Cathepsin D (Fig. 3E) was present at the expected 33 kDa.[47] Cathepsin G (Fig. 3F) was not detected in any cell line.
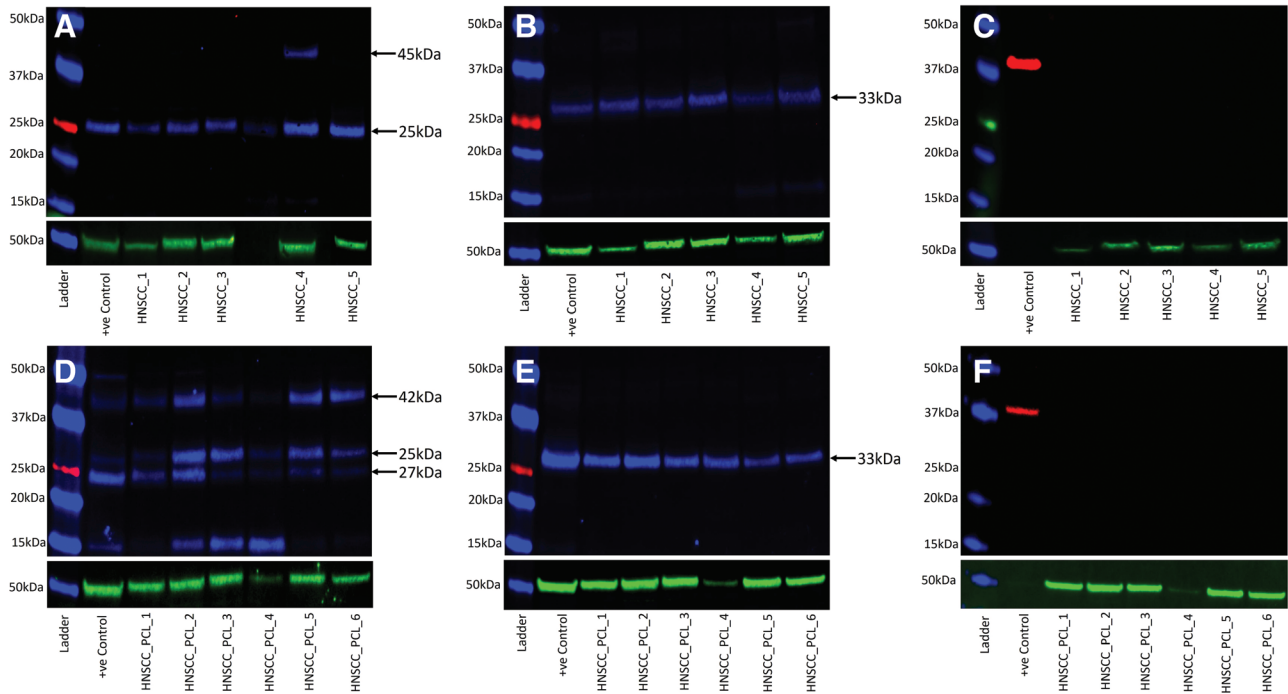
5

Fig. 3. Western blot images of separated total protein extracts from moderately differentiated head and neck cutaneous squamous cell carcinoma (MDHNcSCC) tissue samples (A–C) and MDHNcSCC-derived primary cell lines (D–F), probed for cathepsin B (A, D, blue), cathepsin D (B, E, blue), and cathepsin G (C, F, red), detected with goat anti-rabbit Alexa Fluor 647 (A, D), chicken anti-goat Alex Fluor 647 (B, E), rabbit anti-goat HRP (C), and goat anti-rabbit HRP (F). α-Tubulin (A–F, green) was used as a loading control and detected using goat anti-mouse Alexa Fluor 488.
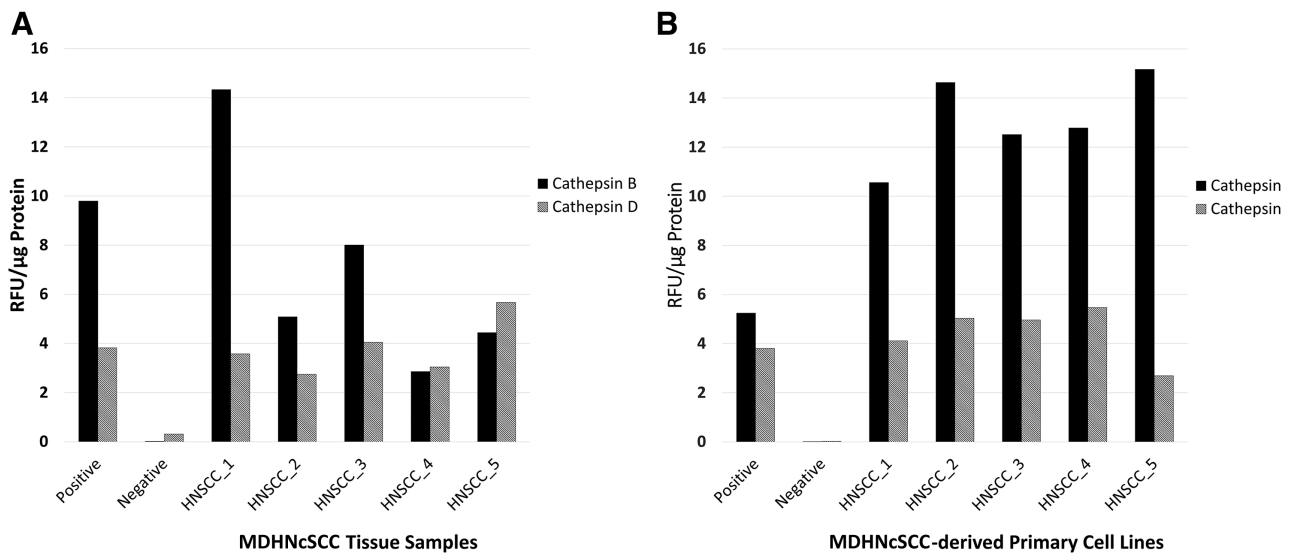

Fig. 4. Enzymatic activity assays of moderately differentiated head and neck cutaneous squamous cell carcinoma (MDHNcSCC) tissue samples (A) and MDHNcSCC-derived primary cell lines (B) for cathepsin B and cathepsin D, with a tonsil as positive control and a denatured tonsil as negative control. RFU, relative fluorescence units.

Positive controls of human tonsil for cathepsins B and D, and a recombinant protein for cathepsin G for both MDHNcSCC tissue samples and MDHNcSCC-derived primary cell lines demonstrated the expected banding. Housekeeper protein α-tubulin (Fig. 3A–F) was detected at the expected molecular weight of 55 kDa and demonstrated approximately equal protein loading and efficient transfer. Negative-control blots for MDHNcSCC tissue samples and MDHNcSCC-derived primary cell lines validated the experiments. [**See figure, Supplemental Digital Content 4**, which shows western blot negative controls of protein extracts from moderately differentiated head and neck squamous cell carcinoma (MDHNcSCC) tissue samples (A) and MDHNcSCC-derived primary cell lines (B).
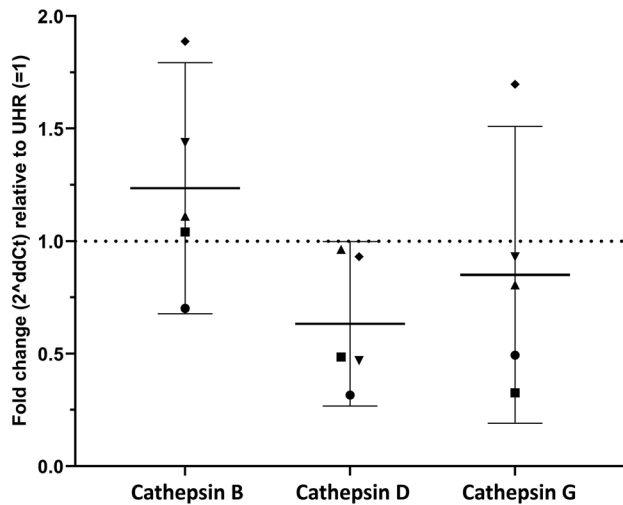
Fig. 5. Transcript expression of cathepsin B, cathepsin D, and cathepsin G in moderately differentiated head and neck cutaneous squamous cell carcinoma tissue samples (A–C). Expression is depicted as fold-change relative to universal human RNA, normalized against housekeeping genes glyceraldehyde 3-phosphate dehydrogenase and Pumilio RNA Binding Family Member 1. The 95% confidence interval of the mean is represented by the error bars.

Controls were performed using matched mouse and rabbit isotype, **http://links.lww.com/PRSGO/B450**.]

Enzymatic Activity Assays

EAAs confirmed the functional activities of cathepsins B and D (Fig. 4A) in all 5 MDHNcSCC tissue samples, with no statistically significant difference between the enzymatic activities of cathepsins B and D in MDHNcSCC tissue samples ($t = 1.156$; $P = 0.312$). EAAs also confirmed functional activities of cathepsins B and D (Fig. 4B) in all 5 MDHNcSCC-derived primary cell lines. Appropriate levels of activity were detected for positive and negative controls. Statistical analysis showed that cathepsin B had a higher enzymatic activity than cathepsin D in the MDHNcSCC-derived primary cell lines ($t = 10.3$; $P < 0.001$).

RT-qPCR

RT-qPCR confirmed transcript expression of cathepsins B, D, and G (Fig. 5) in all 5 MDHNcSCC tissue samples, with the mean level from 5 tissue samples at a level similar to that found in UHR. Electrophoresis of qPCR products on 2% agarose gels confirmed specific amplification of the products. The expected size amplicons were observed, and no products were observed in the no-template-control reactions. [**See figure, Supplemental Digital Content 5**, which shows bands on gel electrophoresis displaying the expected size for PCR products, demonstrating specificity of the probes in MDHNcSCC tissue samples for cathepsin B (A), cathepsin D (B), cathepsin G (C), and the housekeeper genes *GAPDH* (D) and *PUM1* (E), **http://links.lww.com/PRSGO/B451**.]

DISCUSSION

CSCs have been identified in many cancer types, including OCSCC of different subsites,[9–11] glioblastoma,[12] renal clear cell carcinoma,[13] primary[14] and metastatic[15] colon adenocarcinoma, and metastatic malignant melanoma.[16,17] We have recently reported the presence of 4 CSC subpopulations within human MDHNcSCC: an OCT4+/NANOG+/SOX2+/KLF4+/c-MYC+ subpopulation within the TNs, the PTS, the endothelium of the microvessels within the PTS, and an OCT4+/NANOG−/SOX2+/KLF4+/c-MYC+ subpopulation solely within the PTS.[27] These CSCs have been suggested as a novel therapeutic target[5] by modulating the RAS.[25,26]

Recent reports demonstrate the expression of RAS on CSC components in many cancer types, including glioblastoma,[20] oral tongue[21] and buccal mucosal[22] SCC, metastatic colon adenocarcinoma,[15] and metastatic malignant melanoma.[24] Recent literature suggests a key role for the RAS in tumorigenesis,[29–31] with many studies demonstrating a reduced recurrence and overall increased survival of cancer patients who are administered RAS inhibitors.[48,49] We have recently shown the expression of the RAS components: PRR, ACE, AT$_1$R, and AT$_2$R by these CSC subpopulations in MDHNcSCC.[28]

This study demonstrates the novel findings of cathepsins B, D, and G, which constitute a bypass loop for the RAS, by these CSC subpopulations, further providing insight into the biology of MDHNcSCC.

Cathepsins B and D are expressed by the c-MYC+ CSC subpopulations and the OCT4+ CSC subpopulations within the TNs, the PTS, and the endothelium of the microvessels within the PTS of MDHNcSCC. Intriguingly, we also observed an OCT4− population of cells within the PTS that expressed cathepsin B only. The precise nature of these cells requires further investigation. This localization of functionally active cathepsins B and D suggests the presence of RAS bypass loops in these CSCs, similar to IH,[32] glioblastoma,[36] oral tongue SCC,[37] and metastatic colon adenocarcinoma.[38]

Cathepsin G is expressed by the tryptase+ mast cells within the PTS, which also express c-MYC. The finding of transcript expression of cathepsin G in the MDHNcSCC tissue samples but not the MDHNcSCC-derived primary cell lines may be explained by the reduction in cellular heterogeneity by the inadvertent removal of mast cells during culture, as they are nonadherent in vitro.[50] c-MYC in mast cells has been demonstrated to enhance interleukin-3–dependent growth,[51] suggesting that c-MYC expression in these mast cells supports their proliferation in MDHNcSCC. Interestingly, c-MYC expression has been shown to rapidly recruit mast cells required for angiogenesis and macroscopic expansion in a pancreatic islet tumor model.[52]

Inhibitors of cathepsin B,[53] cathepsin D,[54] and cathepsin G[55] currently exist. Curcumin, which inhibits the release of cathepsins B and D from lysosymes,[56] has been proposed as a useful agent in the prevention and treatment of cancer,[57–59] including in HNSCC.[60] Both curcumin and RAS inhibitors have an established safety profile. It is exciting to speculate that combined use of RAS and cathepsin inhibitors may be a novel therapeutic approach to effective targeting of CSCs in the treatment of this common cancer.

LIMITATIONS AND FUTURE DIRECTIONS

The findings of this study are novel and provide insights into the pathogenesis of HNcSCC. Further work with a larger sample size and functional experiments will be needed to confirm the functional role of cathepsins including their roles in bypass loops of the RAS, in regulating CSCs in this tumor. Although immunohistochemical staining of MDHNcSCC tissues displayed a spatial distribution of cells (including tumor cells and those present in the tumor microenvironment), these cells could not be differentiated in WB, RT-qPCR, and EAAs. Analysis of MDHNcSCC-derived primary cell lines was used to overcome this limitation because the cell lines may be more representative of the CSC subpopulations and tumor cells.

Swee T. Tan, MBBS, FRACS, PhD
Gillies McIndoe Research Institute
PO Box 7184
Newtown
Wellington 6242
New Zealand
E-mail: swee.tan@gmri.org.nz

REFERENCES

1. Brougham ND, Dennett ER, Cameron R, et al. The incidence of metastasis from cutaneous squamous cell carcinoma and the impact of its risk factors. *J Surg Oncol.* 2012;106:811–815.
2. Alam M, Ratner D. Cutaneous squamous-cell carcinoma. *N Engl J Med.* 2001;344:975–983.
3. Ch'ng S, Maitra A, Allison RS, et al. Parotid and cervical nodal status predict prognosis for patients with head and neck metastatic cutaneous squamous cell carcinoma. *J Surg Oncol.* 2008;98:101–105.
4. Han J, Fujisawa T, Husain SR, et al. Identification and characterization of cancer stem cells in human head and neck squamous cell carcinoma. *BMC Cancer.* 2014;14:173.
5. Krishnamurthy S, Nör JE. Head and neck cancer stem cells. *J Dent Res.* 2012;91:334–340.
6. Bradshaw A, Wickremsekera A, Tan ST, et al. Cancer stem cell hierarchy in glioblastoma multiforme. *Front Surg.* 2016;3:21.
7. Koh SP, Wickremesekera AC, Itinteang T, et al. Fate mapping of human glioblastoma reveals an invariant stem cell hierarchy. *Transl Cancer Res.* 2018;7(S4):S476–S479.
8. O'Connor ML, Xiang D, Shigdar S, et al. Cancer stem cells: a contentious hypothesis now moving forward. *Cancer Lett.* 2014;344:180–187.
9. Yu HH, Featherston T, Tan ST, et al. Characterization of cancer stem cells in moderately differentiated buccal mucosal squamous cell carcinoma. *Front Surg.* 2016;3:46.
10. Ram R, Brasch HD, Dunne JC, et al. The identification of three cancer stem cell subpopulations within moderately differentiated lip squamous cell carcinoma. *Front Surg.* 2017;4:12.
11. Baillie R, Itinteang T, Yu HH, et al. Cancer stem cells in moderately differentiated oral tongue squamous cell carcinoma. *J Clin Pathol.* 2016;69:742–744.
12. Bradshaw A, Wickremesekera A, Brasch HD, et al. Cancer stem cells in glioblastoma multiforme. *Front Surg.* 2016;3:48.
13. Cane R, Kennedy-Smith A, Brasch H, et al. Characterization of cancer stem cells in renal clear cell carcinoma. *J Stem Cell Regen Biol.* 2019;5:6–17.
14. Munro MJ, Wickremesekera SK, Peng L, et al. Cancer stem cell subpopulations in primary colon adenocarcinoma. *PLoS One.* 2019;14:e0221963.
15. Narayanan A, Wickremesekera SK, Van Schaijik B, et al. Cancer stem cells in liver metastasis from colon adenocarcinoma express components of the renin-angiotensin system. *J Cancer Metastasis Treat.* 2019;5:36
16. Wickremesekera AC, Brasch HD, Lee VM, et al. Expression of cancer stem cell markers in metastatic melanoma to the brain. *J Clin Neurosci.* 2019;60:112–116.
17. Yoganandarajah V, Patel J, van Schaijik B, et al. Identification of cancer stem cell subpopulations in head and neck metastatic malignant melanoma. *Cells.* 2020;9:324.
18. Yang L, Shi P, Zhao G, et al. Targeting cancer stem cell pathways for cancer therapy. *Signal Transduct Target Ther.* 2020;5:8.
19. Desai A, Yan Y, Gerson SL. Concise reviews: cancer stem cell targeted therapies: toward clinical success. *Stem Cells Transl Med.* 2019;8:75–81.
20. Bradshaw AR, Wickremesekera AC, Brasch HD, et al. Glioblastoma multiforme cancer stem cells express components of the renin–angiotensin system. *Front Surg.* 2016;3:51.
21. Itinteang T, Dunne JC, Chibnall AM, et al. Cancer stem cells in moderately differentiated oral tongue squamous cell carcinoma express components of the renin-angiotensin system. *J Clin Pathol.* 2016;69:942–945.
22. Featherston T, Yu HH, Dunne JC, et al. Cancer stem cells in moderately differentiated buccal mucosal squamous cell carcinoma express components of the renin–angiotensin system. *Front Surg.* 2016;3:52.
23. Ram RS, Brasch HD, Dunne JC, et al.. Cancer stem cells in moderately differentiated lip squamous cell carcinoma express components of the renin–angiotensin system. *Front Surg.* 2017;4:30.
24. Wickremesekera AC, Brasch HD, Lee VM, et al. Cancer stem cell subpopulations in metastatic melanoma to the brain express components of the renin-angiotensin system. *J Cancer Metastasis Treat.* 2019;5:62.
25. Tan D, Roth I, Wickremesekera A, et al. Therapeutic targeting of cancer stem cells in human glioblastoma by manipulating the renin-angiotensin system. *Cells.* 2019;8:1364.
26. Roth IM, Wickremesekera AC, Wickremesekera SK, et al. Therapeutic targeting of cancer stem cells via modulation of the renin-angiotensin system. *Front Oncol.* 2019;9:745.
27. Koh SP, Brasch HD, de Jongh J, et al. Cancer stem cell subpopulations in moderately differentiated head and neck cutaneous squamous cell carcinoma. *Heliyon.* 2019;5:e02257.
28. Nallaiah S, Lee VMY, Brasch HD, et al. Cancer stem cells within moderately differentiated head and neck cutaneous squamous cell carcinoma express components of the renin-angiotensin system. *J Plast Reconstr Aesthetic Surg.* 2019;72:1484–1493.
29. Munro MJ, Wickremesekera AC, Davis PF, et al. Renin-angiotensin system and cancer: a review. *Integr Cancer Sci Ther.* 2017;4:1–6.
30. Ager EI, Neo J, Christophi C. The renin-angiotensin system and malignancy. *Carcinogenesis.* 2008;29:1675–1684.
31. Wegman-Ostrosky T, Soto-Reyes E, Vidal-Millán S, et al. The renin-angiotensin system meets the hallmarks of cancer. *J Renin Angiotensin Aldosterone Syst.* 2015;16:227–233.
32. Itinteang T, Chudakova DA, Dunne JC, et al. Expression of cathepsins B, D, and G in infantile hemangioma. *Front Surg.* 2015;2:26.
33. Neves FA, Duncan KG, Baxter JD. Cathepsin B is a prorenin processing enzyme. *Hypertension.* 1996;27(3 Pt 2):514–517.

34. Naseem RH, Hedegard W, Henry TD, et al. Plasma cathepsin D isoforms and their active metabolites increase after myocardial infarction and contribute to plasma renin activity. *Basic Res Cardiol.* 2005;100:139–146.

35. Unger T. The role of the renin-angiotensin system in the development of cardiovascular disease. *Am J Cardiol.* 2002;89(2A):3A–9A; discussion 10A.

36. Koh SP, Wickremesekera AC, Brasch HD, et al. Expression of cathepsins B, D, and G in isocitrate dehydrogenase-wildtype glioblastoma. *Front Surg.* 2017;4:28.

37. Featherston T, Marsh RW, van Schaijik B, et al. Expression and localization of cathepsins B, D, and G in two cancer stem cell subpopulations in moderately differentiated oral tongue squamous cell carcinoma. *Front Med.* 2017;4:100.

38. Mehrotra S, Wickremesekera SK, Brasch HD, et al. Expression and localization of cathepsins B, D and G in cancer stem cells in liver metastasis from colon adenocarcinoma. *Front Surg.* 2018;5:40.

39. Ratna A, Das SK. Role of cathepsins, in particular cathepsins B and D in breast cancer: mechanisms and clinical implications. In: Chakraborti S, Dhalla NS, eds. *Pathophysiological Aspects of Proteases.* Singapore: Springer Singapore; 2017:171–189.

40. Fonović M, Turk B. Cysteine cathepsins and their potential in clinical therapy and biomarker discovery. *Proteomics Clin Appl.* 2014;8:416–426.

41. Zeillinger R, Eder S, Schneeberger C, et al. Cathepsin D and PAI-1 expression in human head and neck cancer. *Anticancer Res.* 1996;16:449–453.

42. Yang X, Wei KJ, Zhang L, et al. Increased expression of cathepsin B in oral squamous cell carcinoma. *Int J Oral Maxillofac Surg.* 2010;39:174–181.

43. Chowdhury A, Romaniello D, Ghosh S, et al. Protease, an advance therapeutic target in cancer. In: Chakraborti S, Dhalla NS, eds. *Pathophysiological Aspects of Proteases.* Singapore: Springer Singapore; 2017:297–317.

44. Crocker J, Jenkins R, Burnett D. Immunohistochemical localization of cathepsin G in human tissues. *Am J Surg Pathol.* 1985;9:338–343.

45. Paterson C, Lee VMY, Brasch HD, et al. Expression of cathepsins B, D and G by the embryonic stem cell-like population within human keloid tissues and keloid-derived primary cell Lines. *Plast Reconstr Surg.* 2019;144:1338–1349.

46. Kingham PJ, Pocock JM. Microglial secreted cathepsin B induces neuronal apoptosis. *J Neurochem.* 2001;76:1475–1484.

47. Sender V, Moulakakis C, Stamme C. Pulmonary surfactant protein A enhances endolysosomal trafficking in alveolar macrophages through regulation of Rab7. *J Immunol.* 2011;186:2397–2411.

48. Sun H, Li T, Zhuang R, Cai W, et al. Do renin-angiotensin system inhibitors influence the recurrence, metastasis, and survival in cancer patients?: evidence from a meta-analysis including 55 studies. *Medicine.* 2017;96:e6394.

49. McKay RR, Rodriguez GE, Lin X, et al. Angiotensin system inhibitors and survival outcomes in patients with metastatic renal cell carcinoma. *Clin Cancer Res.* 2015;21:2471–2479.

50. Yamada N, Matsushima H, Tagaya Y, et al. Generation of a large number of connective tissue type mast cells by culture of murine fetal skin cells. *J Invest Dermatol.* 2003;121:1425–1432.

51. Hume CR, Nocka KH, Sorrentino V, et al. Constitutive c-myc expression enhances the response of murine mast cells to IL-3, but does not eliminate their requirement for growth factors. *Oncogene.* 1988;2:223–226.

52. Soucek L, Lawlor ER, Soto D, et al. Mast cells are required for angiogenesis and macroscopic expansion of Myc-induced pancreatic islet tumors. *Nat Med.* 2007;13:1211–1218.

53. Li YY, Fang J, Ao GZ. Cathepsin B and L inhibitors: a patent review (2010 - present). *Expert Opin Ther Pat.* 2017;27: 643–656.

54. Dumas J, Brittelli D, Chen J, et al. Synthesis and structure activity relationships of novel small molecule cathepsin D inhibitors. *Bioorg Med Chem Lett.* 1999;9:2531–2536.

55. Greco MN, Hawkins MJ, Powell ET, et al. Nonpeptide inhibitors of cathepsin G: optimization of a novel beta-ketophosphonic acid lead by structure-based drug design. *J Am Chem Soc.* 2002;124:3810–3811.

56. Nirmala C, Puvanakrishnan R. Effect of curcumin on certain lysosomal hydrolases in isoproterenol-induced myocardial infarction in rats. *Biochem Pharmacol.* 1996;51:47–51.

57. Lampe CM, Gondi CS. Cathepsin B inhibitors for targeted cancer therapy. *J Cancer Sci Ther.* 2014;6:10.

58. Tomeh M, Hadianamrei R, Zhao X. A review of curcumin and its derivatives as anticancer agents. *Int J Mol Sci.* 2019;20:1033.

59. Ravindran J, Prasad S, Aggarwal BB. Curcumin and cancer cells: how many ways can curry kill tumor cells selectively? *AAPS J.* 2009;11:495–510.

60. Wilken R, Veena MS, Wang MB, et al. Curcumin: a review of anti-cancer properties and therapeutic activity in head and neck squamous cell carcinoma. *Mol Cancer.* 2011;10:12.